Acta Pharmaceutica Sinica B 2021;11(12):4020–4031

Chinese Pharmaceutical Association
Institute of Materia Medica, Chinese Academy of Medical Sciences

Acta Pharmaceutica Sinica B

www.elsevier.com/locate/apsb
www.sciencedirect.com

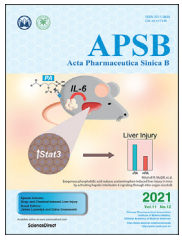

ORIGINAL ARTICLE

Target-responsive subcellular catabolism analysis for early-stage antibody–drug conjugates screening and assessment

Hua Sang[a,b,†], Jiali Liu[a,†], Fang Zhou[a], Xiaofang Zhang[a], Jingwei Zhang[a], Yazhong Liu[a], Guangji Wang[a,*], Hui Ye[a,*]

[a]*Jiangsu Provincial Key Laboratory of Drug Metabolism and Pharmacokinetics, State Key Laboratory of Natural Medicines, China Pharmaceutical University, Nanjing 210009, China*
[b]*Department of Pharmacy, the Affiliated Hospital of Nantong University, Nantong 226001, China*

Received 2 April 2021; received in revised form 8 May 2021; accepted 18 May 2021

KEY WORDS

ADC;
Target-responsive subcellular catabolism (TARSC);
T-DM1;
Therapeutic efficacy;
Screening;
Biosimilarity

Abstract Events including antibody–antigen affinity, internalization, trafficking and lysosomal proteolysis combinatorially determine the efficiency of antibody–drug conjugate (ADC) catabolism and hence the toxicity. Nevertheless, an approach that conveniently identifies proteins requisite for payload release and the ensuing toxicity for mechanistic studies and quality assessment is lacking. Considering the plethora of ADC candidates under development, we developed a target-responsive subcellular catabolism (TARSC) approach that examines ADC catabolism and probes changes in response to targeted interferences of proteins of interest. We firstly applied TARSC to study the commercial T-DM1 and the biosimilar. We recorded unequivocal catabolic behaviors regardless of the absence and presence of the targeted interferences. Their negligible differences in TARSC profiles agreed with their undifferentiated anti-tumoral efficacy according to further *in vitro* viability and *in vivo* tumor growth assays, highlighting TARSC analysis as a useful tool for biosimilarity assessment and functional dissection of proteins requisite for ADC catabolism. Additionally, we employed TARSC to investigate the catabolic behavior of a new trastuzumab–toxin conjugate. Collectively, TARSC can not only characterize ADC catabolism at (sub)cellular level but also comprehensively determine which protein targets affect payload release and therapeutic outcomes. Future use of TARSC is thus anticipated in early-stage screening, quality assessment and mechanistic investigations of ADCs.

*Corresponding authors. Tel.: +86 25 83271176 (Guangji Wang), +86 25 83271179 (Hui Ye)
E-mail addresses: guangjiwang@hotmail.com (Guangji Wang), cpuyehui@cpu.edu.cn (Hui Ye).
[†]These authors made equal contributions to this work.
Peer review under responsibility of Chinese Pharmaceutical Association and Institute of Materia Medica, Chinese Academy of Medical Sciences.

https://doi.org/10.1016/j.apsb.2021.05.024

1. Introduction

Antibody−drug conjugates (ADCs) consist of monoclonal antibodies (mAbs) conjugated with cytotoxic drugs through linkers. The mAbs carry ADCs to target cells by affinity binding to antigens expressed on cell surface, and subsequently become internalized, undergo degradation followed by the release of toxic payloads within target cells. This design confers increased specificity and reduced toxicity compared to conventional pharmaceutics such as genotoxic drugs[1−3].

As a novel class of therapeutics, ADCs are embracing ever-evolving technologies in linker and payload chemistry. Specifically, linkers can be classified as cleavable chemical spacers involving hydrozone, disulfide and di/tri/tetra-peptide bonds and noncleavable spacers such as thioether and pyrophosphate diester[4]. The differences in chemical stability conferred by linkers lead to varied catabolic profiles and hence ADC therapeutic efficacies in target cells or organelles. Moreover, highly potent cytotoxic agents with defined mechanisms of action such as maytansinoid and auristatin with microtubule inhibitory functions or DNA double-strand breakers, cross-linkers and alkylators are often selected as payloads[5]. In addition, the site of conjugation, lysine or cysteine residues, also affects ADC catabolic and pharmacokinetic liabilities[6]. Collectively, the plethora of choices offered by conjugation site, linkers and payloads confers versatile combinations, leading to currently over 100 ADCs in clinical trials and numerous ADCs as preclinical candidates[7,8].

Therefore, the concomitant task of druggability screening and quality assessment for ADC candidates becomes challenging, necessitating an approach that efficiently and comprehensively evaluates ADC attributes before proceeding to expensive and time-consuming *in vivo* experiments[8,9]. Nevertheless, conventional *in vitro* assaying techniques such as cytotoxicity assay merely provides a final functional readout while lacking a comprehensive evaluation of how each step ranging from antigen binding, internalization, trafficking to lysosomal proteolysis-mediated payload release functions and affects payload release and the ensuing cell killing effect[4]. Conventionally, each step described above has often been studied separately. For instance, internalization rate and extent can be screened by flow cytometry and visualized by fluorescent microscopy[10−12]. Moreover, linker stability and lysosomal proteolysis is assessed by monitoring payload release *via* LC–MS/MS after incubating ADCs with miscellaneous proteolytic enzymes such as cathepsin B[13], rat lysosomal lysate[14] and acidified S9 fractions[15]. Nevertheless, a holistic landscape of how each protein target or pathway affects ADC catabolism and consequently the kinetics of catabolic payload is still lacking, albeit it is agreed that such information is of paramount importance in assessing ADC safety and efficacy, and allows identification of proteins that affect ADC catabolism and consequently the toxicity.

Thus, herein we propose a target-responsive subcellular catabolism (TARSC) approach that monitors ADC catabolites kinetics in cancer cells and organelles, and examine the changed kinetics of catabolites in response to targeted interferences of given proteins. TARSC is useful for qualitative and quantitative assessment of ADC payload release, and allows us to determine the involvement of specific targeted proteins to the catabolism profile and therapeutic efficacy of ADCs. We can thus use the gained information to judge the comparability between ADC biosimilars and innovators of interest. In this study, we employed a commercial T-DM1 and its biosimilar as model ADCs, and measured their catabolic behaviors in both the target organelles, lysosomes, and the target cells, HER2-overexpressing BT474 cells. Then, we pharmacologically and genetically interfered with key proteins involved in T-DM1 delivery and catabolism including clathrin-mediated endocytosis, endosome/lysosome transport and lysosomal cathepsin–dependent proteolysis, and recorded significantly impaired production of the toxic payloads as expected. Further, we evaluated their TARSC responses by measuring the payload kinetics for the T-DM1 biosimilar (BS) and its innovator reference (IN) following targeted interferences, and noted unequivocal changes between the BS and IN T-DM1. The negligible differences of the TARSC profiles of the two T-DM1s agree with their undifferentiated therapeutic outcomes suggested by *in vitro* viability assays and *in vivo* tumor growth assays, highlighting the close association of ADC payload kinetics with therapeutic efficacy. Therefore, TARSC can potentially serve as an indicator of therapeutic efficacy and complement with conventional *in vitro* and *in vivo* anti-tumoral assays. Lastly, besides judging the biosimilarity between ADC biosimilar and innovator, we demonstrated the use of TARSC in appraising the payload release efficiency for a new trastuzumab−toxin conjugate that employs different linker chemistry from T-DM1. Collectively, TARSC analysis allows us to characterize ADC catabolism at cellular and subcellular level, and systematically depicts whether given target proteins affect ADC delivery and payload release. Such information is anticipated to support early-stage ADC screening, quality assessment and mechanistic understanding for ADC candidates during drug R&D before proceeding to costly and time-consuming *in vivo* experiments.

2. Materials and methods

2.1. Chemicals and reagents

The commercially available trastuzumab (T)-DM1 was purchased from Hoffmann-La Roche Inc. (Basel, Switzerland), and the BS trastuzumab-DM1 was manufactured by Shanghai Hengrui Pharmaceutical Co., Ltd. (Shanghai, China) as previously detailed[16]. The ADC DX-006 was kindly provided by Hangzhou DAC Biotech Co., Ltd. (Hangzhou, China). Chloropromazine, E64d, CA-074 methyl ester (CA-074-ME), pepstatin A, aprotinin and tris (2-carboxyethyl) phosphine hydrochloride (TCEP) were purchased from Sigma−Aldrich (St. Louis, MO, USA). Bafilomycin A1 was purchased from Selleck Chemicals (Houston, TX, USA). Ansamitocin P-3 was purchased from Medchem Express (Monmouth Junction, NJ, USA). Cell Counting Kit-8 (CCK-8) was purchased

from Beyotime (Nanjing, China). Monoclonal antibody against HER2 (Cat#AB16901) was purchased from Abcam (Cambridge, MA, USA). Rhodamine Red™-X (RRX) AffiniPure Donkey Anti-Mouse IgG (H + L) was purchased from Jackson ImmunoResearch Laboratories Inc. (Philadelphia, PA, USA). Acetonitrile (ACN, HPLC-grade) was purchased from Merck (Darmstadt, Germany). Deionized water was prepared by Milli-Q system (Millipore, Billerica, MA, USA). All other reagents and solvents were purchased from Sigma−Aldrich and of analytical grade.

2.2. Cell culture

Human breast cancer cells BT474 was purchased from the American Type Culture Collection. The cells (passages 8 to 25) were cultured in RPMI 1640 medium supplemented with 10% fetal bovine serum and 100 U/mL penicillin and streptomycin (Invitrogen, Carlsbad, CA, USA) at 37 °C with 5% CO_2. The medium was changed every other day.

2.3. Animals

All animal care and experimental procedures were conducted according to the National Research Council's Guidelines for the Care and Use of Laboratory Animals and were approved by the SPF Animal Laboratory of China Pharmaceutical University (Animal authorization reference number: SYXK2016-0011). Healthy female BALB/c nude mice (18−22 g of weight and 6−8 weeks of age) were obtained from Shanghai SLAC Laboratory Animal Co., Ltd. (Shanghai, China). The mice were maintained under controlled environment (22−24 °C, 50%−60% humidity, 12-h light/12-h dark cycle) with *ad libitum* access to standard laboratory food and water.

2.4. Lysosomal target-responsive subcellular catabolism analysis

Lysosomal subcellular catabolism analysis of ADCs was conducted by first incubating the ADCs with crude lysosome fractions (CLF). The CLF derived from rat liver was prepared according to the manufactures' instructions using a Lysosome Isolation Kit (LYSISO1, Sigma−Aldrich). Briefly, fresh liver tissue was harvested from fasted rats, washed with ice-cold PBS and then cut into small slices. The liver slices were then homogenized with 4 volumes of the 1× extraction buffer per gram of tissue, and then the resultant floating fat layer was removed following centrifugation at 1000×*g* for 10 min at 4 °C. The supernatant was transferred to another tube and re-homogenized in 2 volumes of 1× extraction buffer. Then, the supernatant was combined with the previously collected supernatants. The combined supernatant was centrifuged again at 20,000×*g* for 20 min at 4 °C, and then the pellet was collected. The CLF was prepared by resuspension of the pellet in a minimal volume of 1× extraction buffer.

Lysosomal activity of prepared CLF was examined using the Acid Phosphatase Assay Kit (CS0740, Sigma−Aldrich). Briefly, substrate solution was freshly prepared by dissolving one 4-nitrophenly phosphate tablet in 2.5 mL of the citrate buffer solution. Then, 50 μL of the CLF was incubated with 50 μL of the substrate solution for 10 min at 37 °C. A blank reaction (substrate solution without enzyme) was run in parallel to account for the 4-nitrophenyl phosphate that becomes hydrolyzed during the incubation. The reaction was terminated by adding 0.2 mL of the stop solution. The colored solution was formed after the addition of 0.5 mol/L NaOH. The absorbance of the mixture was detected at 405 nm.

For the IN and BS T-DM1, incubation of both ADCs with CLF was carried out at 37 °C in a final volume of 100 μL containing 15 μL of CLF, 75 μL of 50 mmol/L ammonium acetate buffer (pH 5.0, with 2 mmol/L TCEP) and 10 μL of ADC prepared in 25 mol/L for 0, 1, 3, 6, 12, 24, 48, 72, 96 and 120 h. After incubation for different duration, the resultant ADC catabolites was determined by LC–MS/MS-based quantitative analysis as described in the following section, and the kinetic profiles of ADC catabolites abundance were plotted against incubation time. To perform the lysosomal TARSC analysis for IN and BS T-DM1s, we specifically examined the contribution of given lysosomal enzymes to ADC payload release by co-incubating the protease inhibitors with ADCs in CLF followed by quantitative analysis of the produced catabolites. The assayed protease inhibitors include cysteine protease inhibitors (CA-074-ME and E64d at 10 μmol/L), a serine protease inhibitor (aprotinin at 20 μg/mL) and an aspartic protease inhibitor (pepstatin A at 10 μg/mL). Inhibition was terminated at 24, 48, 72 and 96 h, respectively, by adding 400 μL of ice-cold acetonitrile containing 200 ng/mL ansamitocin P-3 as the internal standard (IS) for subsequent LC–MS/MS analysis. The mixtures were vortexed thoroughly followed by centrifugation at 30,000×*g* for 10 min. The supernatants were collected, dried at room temperature, reconstituted in 100 μL acetonitrile–water (1:1, *v*/*v*). The reconstituted samples were centrifuged at 30,000×*g* for 10 min at 4 °C and a 75 μL of supernatant was collected for subsequent LC–MS/MS analysis.

For DX-006, the incubation of ADCs with CLF was carried out at 37 °C in a final volume of 100 μL containing 15 μL of CLF, 75 μL of 50 mmol/L ammonium acetate buffer (pH 5.0, with 2 mmol/L TCEP) and 10 μL of DX-006 prepared in 100 nmol/L for 0, 1, 2, 4, 6, 12, 24, 48, 72, 96 and 120 h. After incubation for different duration, the resultant catabolites of DX-006 was determined by LC–MS/MS-based quantitative analysis as described in following section, and the kinetic profiles of ADC catabolites abundance were plotted against incubation duration.

To perform the lysosomal TARSC analysis for DX-006, we co-administrated DX-006 with specific cysteine proteases inhibitors (10 μmol/L E64d, 10 μmol/L CA-074-ME) for 48 h, the influence of given lysosomal enzymes on DX-006 payload release was determined by quantitative analysis of the produced catabolites.

2.5. Target-responsive subcellular catabolism analysis

BT474 cells were treated with an IN T-DM1 and a BS T-DM1 at different concentrations (12.5, 25, and 50 nmol/L), respectively. At different intervals post-administration, BT474 cells were rinsed with ice-cold PBS and lysed by three freeze−thaw cycles. Protein concentrations were measured by the Bradford assay, and the concentration of the main catabolites of T-DM1, DM1 and lys-MCC-DM1 were determined by LC–MS/MS (described below).

To conduct the TARSC analysis, given proteins involved in ADC delivery and payload release in cells were interfered by siRNA or specific inhibitors before ADC treatment. Specifically, HER2 was pre-silenced by transfecting the BT474 cells with siRNA for 48 h according to the procedures described below in the *HER2* knockdown section. Moreover, clathrin-mediated internalization was inhibited by pre-incubating the BT474 cells with chlorpromazine at 10 μmol/L for 2 h, and the H^+-ATPase activity

was impaired by pre-administering 1 nmol/L Bafilomycin A1 to cells for 2 h. For lysosomal proteases, 3 μmol/L CA-074-ME and 20 μmol/L E64d were pre-administered for 2 h to inhibit the activity of cysteine proteases, whereas 20 μg/mL aprotinin and pepstatin A were pre-administered for 2 h to inhibit the activity of serine and aspartic proteases in BT474 cells, respectively. Following the pre-interference, cells were treated with 25 nmol/L IN T-DM1 or BS T-DM1 for another 72 h, respectively. The resultant changes of toxic payloads following the targeted interferences were quantified by LC–MS/MS.

2.6. LC–MS/MS-based quantitative analysis of T-DM1 payloads

The major catabolites of T-DM1, lys-MCC-DM1 and DM1, present in lysosomes, cells and tumor mass were prepared and analyzed on a Shimadzu LC-20 HPLC system (Kyoto, Japan) coupled to QTRAP 5500 (SCIEX, Birmingham, MA, USA). Briefly, catabolites in CLF, cell lysates and tissue homogenates were extracted with 4 times volume of ice-cold ACN containing 200 ng/mL ansamitocin P-3 (IS). After centrifugation (30,000×*g*, 10 min, 4 °C), the supernatants were collected and evaporated to dryness with nitrogen at room temperature followed by reconstitution in 100 μL acetonitrile–water (1:1, *v*/*v*). The reconstituted samples were centrifuged at 30,000×*g* for 10 min at 4 °C before injections onto the LC–MS/MS system.

For analysis of T-DM1 catabolites, chromatographic separation was achieved using a Luna C18 column (100 mm × 2.0 mm, 2.6 μm, Phenomenex, Torrance, CA, USA) at 40 °C on the Shimadzu HPLC. The mobile phase consisted of solvent A (0.1% aqueous formic acid) and solvent B (acetonitrile with 0.1% formic acid), and a 11-min gradient was used: 0 min, 20% B; 0.5 min, 20% B; 5.5 min, 100% B; 8.5 min, 20% B; 11 min, 20% B with a flow rate of 0.2 mL/min. Following separation, QTRAP 5500 was operated in the positive electrospray ionization (ESI) mode for the quantitative analysis of T-DM1 payloads. Briefly, the multiple reaction monitoring (MRM) parameters employed on the QTRAP were set as follows: declustering potential set at 60 V for lys-MCC-DM1, DM1 and IS, collision energy set at 55 eV for lys-MCC-DM1, 33 eV for DM1 and 40 eV for the IS, MRM transitions set as *m*/*z* 1103.7 → 485.2 for lys-MCC-DM1, *m*/*z* 738.5 → 547.4 for DM1, *m*/*z* 635.5 → 547.3 for the IS. Data acquisition and analysis were both performed using Analyst TF 1.5.1 software (SCIEX, Birmingham, MA, USA). The LC–MS/MS-based quantitative method of T-DM1 payloads has been validated as we previously published[17].

For analysis of DX-006 catabolites, chromatographic separation was achieved using a Luna C18 column (100 mm × 2.0 mm, 2.6 μm, Phenomenex, Torrance, CA, USA) at 40 °C on HPLC (Shimadzu). The mobile phase consisted of solvent A (0.1% aqueous formic acid) and solvent B (acetonitrile with 0.1% formic acid). A 10-min gradient was used as follows: 0 min, 10% B; 2 min, 10% B; 4 min, 95% B; 7 min, 95% B; 7.5 min, 10% B; 10 min, 10% B with a flow rate of 0.2 mL/min. Following separation, QTRAP 5500 was operated in the positive ESI mode for the quantitative analysis of T-DM1 payloads. Briefly, the MRM parameters employed on the QTRAP were set as follows: declustering potential set at 60 V for cys-Tub-006, Tub-006 and IS, collision energy set at 40 eV for cys-Tub-006, Tub-006 and IS, MRM transitions set as *m*/*z* 1033.7 → 807.3 for cys-Tub-006, *m*/*z* 912.5 → 686.3 for DM1, *m*/*z* 635.5 → 547.3 for the IS. Data acquisition and analysis were both performed using Analyst TF 1.5.1 software.

2.7. HER2 knockdown

HER2 was silenced by transfecting the BT474 cells upon plating with 10 nmol/L small interfering RNA (siRNA) (5′-GGA CAC GAU UUU GUG GAA Gtt-3′) or 10 nmol/L scrambled siRNA using Lipofectamine® RNAiMAX (Life Technologies, Carlsbad, CA, USA). The RNAi duplex–Lipofectamine® RNAiMAX complexes were prepared and then mixed with the appropriate number of BT474 cells when plating. After 48 h, HER2 silencing efficiency was confirmed by flow cytometry and immunofluorescence staining. Briefly, cells administered with scrambled siRNA or siRNA targeting HER2 were fixed with 4% polyformaldehyde solution. After washing and blocking with 5% bovine serum albumin, cells were incubated with anti-HER2 (1:100) at 4 °C overnight and then incubated with Rhodamine-conjugated secondary antibody (1:200) at 37 °C for 1 h. Following additional washing, the fluorescently labeled cells were loading onto BD Accuri™ C6 plus flow cytometer (San Jose, CA, USA) for quantitative analysis and imaged with an Olympus FV3000 confocal microscope (Shinjuku, Japan) for qualitative analysis.

2.8. In vitro cell growth inhibition assay

BT474 cells was exposed to a series of concentrations of T-DM1 (0.01, 0.05, 0.2, 1, 2.5, 4, 10, 25, and 100 nmol/L), cys-Tub-006 (0.5, 1, 2, 5, 10, 20, 50, 100, 200, and 500 nmol/L) or Tub-006 (0.5, 1, 2, 5, 10, 20, 50, 100, 200, and 500 nmol/L) for 120 h at 37 °C with 5% CO_2. After treatment, cell viabilities were measured using a CCK-8 Assay Kit and quantified by comparing the resultant viabilities with those in the absence of T-DM1 exposure. IC_{50} values were calculated *via* GraphPad Prism 7 (GraphPad Software Inc., San Diego, CA, USA).

To evaluate the contribution of given protein "targets" possibly involved in T-DM1 catabolism to its cytotoxicity, the change of cell survival rate was examined after the targeted interference. Briefly, BT474 cells were exposed to 100 nmol/L IN or BS T-DM1, following 48 h-HER2 pre-silencing or co-administration with 10 μmol/L chlorpromazine, 1 nmol/L Bafilomycin A1, 3 μmol/L CA-074-ME, 20 μmol/L E64d, 20 μg/mL aprotinin and 20 μg/mL pepstatin A, respectively. At 72 h post-T-DM1 exposure, cell viabilities were measured using a CCK-8 Assay Kit and quantified by comparing the resultant viabilities with those in the absence of drug treatment.

2.9. In vivo tumor growth assay

To evaluate the *in vivo* therapeutic efficacy for the assayed T-DM1, a cell line-derived xenograft model was established. The xenografts were generated by subcutaneous injections of 5×10^6 exponentially growing BT474 cells into the right flank of nude mice. Then, the mice bearing BT474 subcutaneous tumors were randomly assigned to the following three groups and administered with single-dosed T-DM1. The three groups include the control group that were injected with saline (0.01 mL/g, i.v.), the IN T-DM1 group that were injected with the IN T-DM1 (15 mg/kg, i.v.) and the BS T-DM1 group that were injected with BS T-DM1 (15 mg/kg, i.v.). Tumor volume was measured every day post-administration for each animal. On Day 1, 4 and 7 post-administration, the mice were sacrificed and the tumor masses were collected. Tumor masses was weighed and homogenized with deionized H_2O to an approximate concentration of 0.1 g/mL. Then, the homogenates were further processed as described above

in the LC–MS/MS sample preparation section. The intra-tumoral concentrations of lys-MCC-DM1 and DM1 were also quantified as described above.

2.10. Data analysis

All data are presented as mean ± standard error of mean (SEM). Statistical analyses were performed using GraphPad Prism 7. Each continuous variable was analyzed for a normal distribution using the Kolmogorov−Smirnov test, and then statistical analysis was performed using a two-tailed Student's *t*-test or one-way ANOVA assay with Dunnett *post-hoc* test if F was less than 0.05 and there was no significant variance inhomogeneity. Differences were considered significant at $^{*}P < 0.05$, $^{**}P < 0.01$, $^{***}P < 0.001$.

3. Results

3.1. Development of the in vitro TARSC analysis approach for ADCs

TARSC analysis records the kinetic profiles of payload release by LC–MS/MS in target cells or subcellular compartments, and further probes the changes of catabolite kinetics in response to targeted interference of proteins that are essential for ADC delivery and payload release (Fig. 1). Specifically, protein targets subjected to pharmacological or genetic interferences are exemplified by HER2 involved in antigen–mAb recognition, clathrin in ADC internalization, H^{+}-ATPase in ADC trafficking and cathepsin in lysosomal proteolysis. Therefore, the induced changes of payload kinetic profiles in response to the interferences imply the involvement of the assayed target proteins in ADC catabolism and can concomitantly dictate their influence on ADC therapeutic outcomes. In contrast, catabolites kinetics that hold constant upon the targeted interferences thus indicate that the selected proteins hardly contribute to ADC delivery and payload release (Fig. 1).

This differentiating capability has thus warranted diverse applications for TARSC analysis. First, TARSC opens new avenues for ADC biosimilarity assessment. Since ADCs of biosimilarity possess almost identical physicochemical attributes, such ADCs should deliver undistinguishable catabolic kinetic profiles and also display unequivocal TARSC profiles in response to targeted interferences (Figs. 2–4). Comparison of the TARSC profiles is thus expected to become a valuable addition to conventional evaluation assays that judge biosimilarity between IN and BS or simply lot-to-lot variations, for instance, by cytotoxicity (Fig. 5). Secondly, TARSC analysis supports ADC mechanistic studies by allowing dissection of which protein/pathway affects ADC catabolism and hence the cell killing effect (Fig. 6). Lastly, TARSC provides clues for ADC optimization and screening. For instance, when assessing ADC candidates composed of different mAbs or linkers, TARSC elucidates which ADC release the payload most efficiently, which is often positively correlated to its therapeutic efficacy. This would serve as a powerful early-stage screening tool that greatly cuts the time and cost spent on *in vivo* assays, and hence accelerates the ADC R&D process.

3.2. Benchmarking lysosomal TARSC analysis using T-DM1s

We initially employed CLF isolated from rat liver and incubated the IN T-DM1 with the isolated CLF for 0, 1, 3, 6, 24, 48, 72, 96 and 120 h. Sensitive detection of major T-DM1 catabolites was achieved by MRM-based LC–MS/MS analysis. As shown in Fig. 2A, exposure of the IN T-DM1 to CLF delivered a time-dependent production of the T-DM1 catabolite lys-MCC-DM1 for the entire duration (1−120 h). In contrary, the other catabolite that is produced independent of lysosomal degradation and usually observed due to unstable linker chemistry, DM1, was nearly absent, indicating that the examined T-DM1 remains stable without unexpected shedding of payloads in the biological environment of CLF. This is further demonstrated by the significantly large AUC of lys-MCC-DM1 over DM1 following T-DM1 incubation (Fig. 2B).

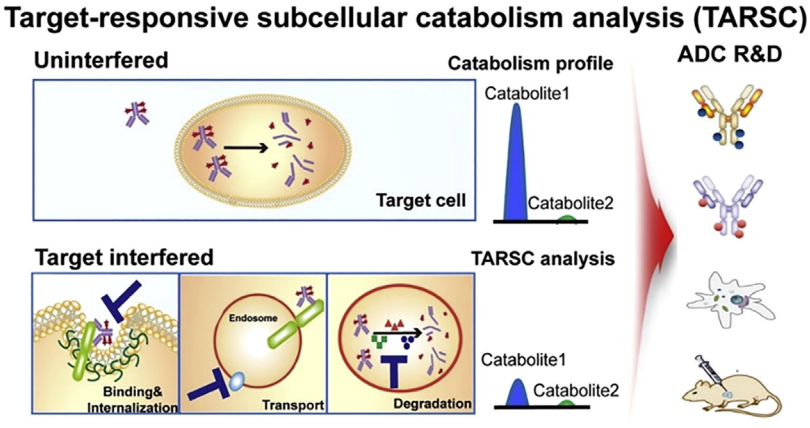

Figure 1 Illustrated workflow of the *in vitro* TARSC approach. TARSC analysis records the kinetic profiles of active payload released from ADCs by LC–MS/MS in target cells or subcellular compartments, and further probes the changes of catabolite kinetics in response to targeted interferences of proteins that potentially affects ADC delivery and payload release. TARSC is anticipated to be a useful tool in ADC R&D. For instance, it opens new avenues for ADC biosimilarity assessment. Since a biosimilar is expected to possess almost identical physicochemical attributes with its innovator reference, it should deliver undistinguishable catabolic behavior and TARSC profile in response to targeted interferences as the innovator. Secondly, TARSC analysis supports ADC mechanistic studies since it conveniently identifies regulators of ADC payload release and hence the toxicity. Thirdly, TARSC is amenable to ADC screening since it examines the ADC candidates that release the toxic payload most efficiently, which is often positively correlated to *in vitro* and *in vivo* therapeutic efficacy.

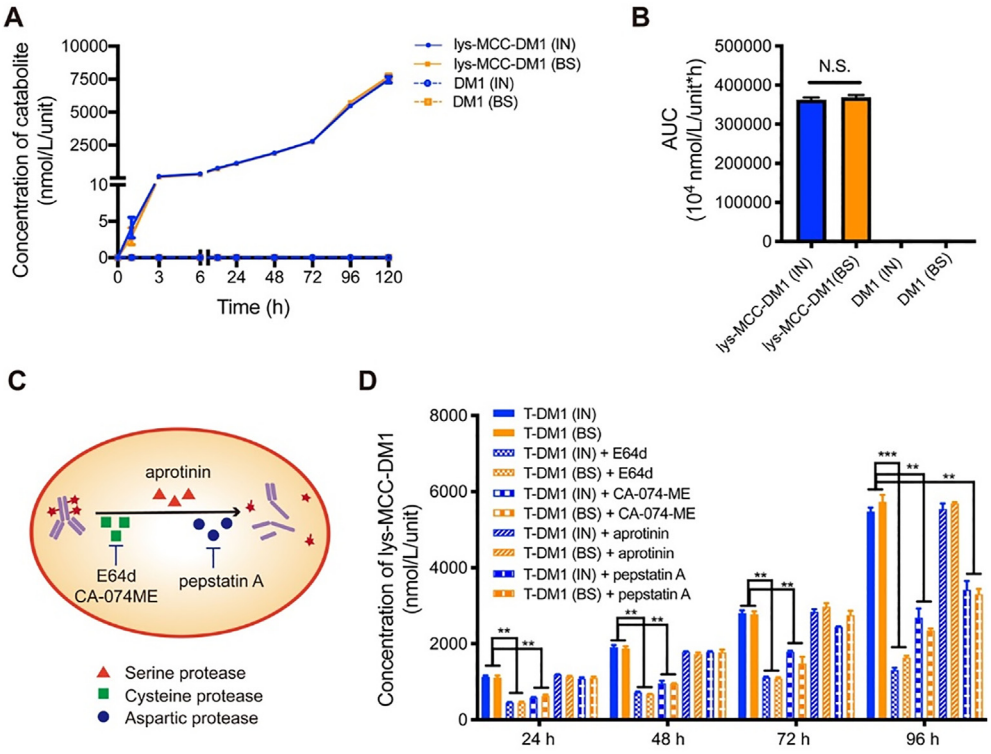

Figure 2 Lysosomal TARSC analysis of the innovator reference (IN) and biosimilar (BS) T-DM1s using rat liver crude lysosome fractions. (A) Catabolic kinetics of T-DM1 after incubation with the crude lysosome fractions isolated from rat liver (25 nmol/L IN *vs.* BS T-DM1, $n = 6$). (B) The areas under curve (AUCs) of the two major catabolites of the IN and BS T-DM1s were compared. (C) Scheme of lysosomal TARSC analysis conducted *via* the administration of specific inhibitors targeting different lysosomal proteases. (D) Influence of given protease inhibitors (10 μmol/L E64d, 10 μmol/L CA-074-ME, 20 μg/mL aprotinin, 10 μg/mL pepstatin A) on the catabolic kinetics of the IN and BS T-DM1s ($n = 6$). All data are presented as mean ± SEM. N.S., no significance, Student's *t*-test for (B) and $^{**}P < 0.01$, $^{***}P < 0.001$, one-way ANOVA for (D).

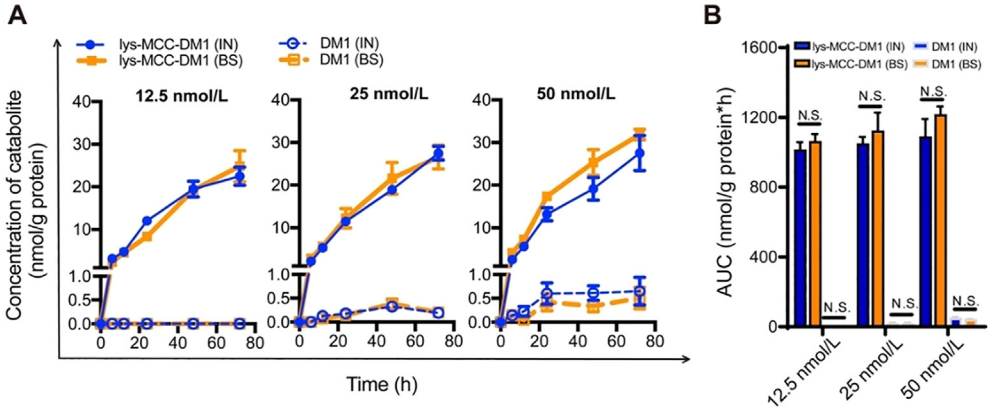

Figure 3 Catabolism profiles of the IN and BS T-DM1s in BT474 cells. (A) Time-resolved kinetic profiles of T-DM1 catabolites in BT474 cells administered with three different doses (12.5, 25 and 50 nmol/L). (B) AUCs of the two major catabolites were compared. Data are expressed as mean ± SEM ($n = 6$). N.S., no significance, Student's *t*-test.

Next, we sought to investigate whether the TARSC analysis allows for determining the lysosomal proteases that are requisite for T-DM1 catabolism. We incubated the CLF with inhibitors targeting different lysosomal proteases including cysteine protease, aspartic proteases and serine protease[18,19] (Fig. 2C), and monitored the post-inhibition kinetic profiles of the two catabolites. We found that the administration of cysteine proteases inhibitors, CA-074-ME and E64d, both significantly reduced the lysosomal concentration of lys-MCC-DM1 when the catabolites were collected at 24, 48, 72 and 96 h (Fig. 2D). In comparison, the inhibitors of aspartic proteases failed to block T-DM1 catabolism until 96 h, whereas the serine protease inhibitor conferred no significant changes to the production of lys-MCC-DM1 at all assayed time points. The distinct outcomes induced by different protease inhibitors are in line with previous knowledge that T-DM1 is cleaved and degraded mainly dependent on cysteine proteases[20].

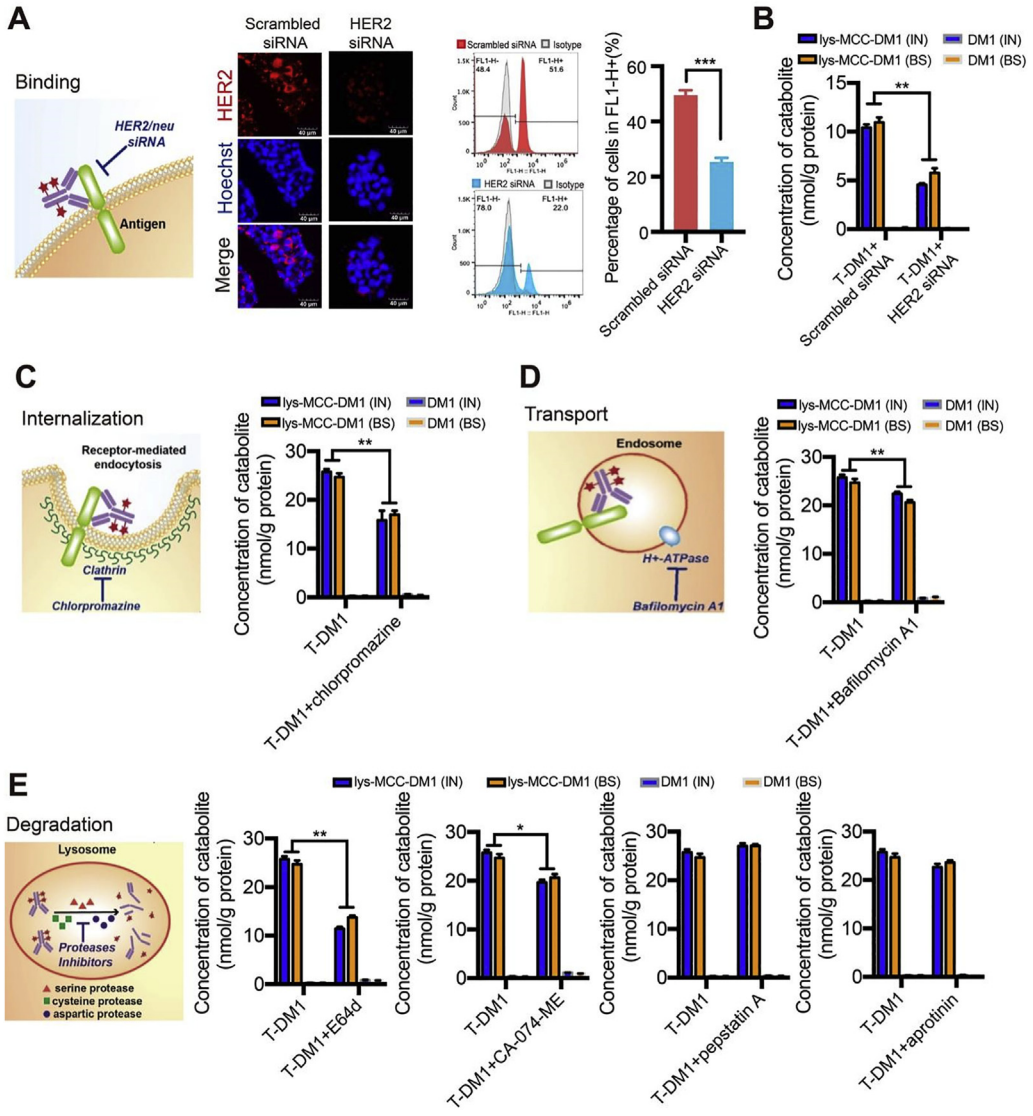

Figure 4 TARSC analysis determines the major catabolic proteins/pathway contributing to the payload release of the IN and BS T-DM1s in BT474 cells. (A) Transfection efficiency of HER2 siRNA in BT474 cells was visualized by immunofluorescence (Red, HER2; Blue, Hoechst) and measured by flow cytometry ($n = 6$). (B) Impact of treatment with HER2 siRNA or scrambled siRNA for 48 h on production of the major T-DM1 catabolites for the IN and BS T-DM1s after incubation for another 72 h. (C) Impact of inhibiting clathrin-dependent internalization with chlorpromazine (10 μmol/L) pre-treatment for 2 h on catabolites produced from the IN and BS T-DM1s with T-DM1 incubation for another 72 h, respectively. (D) Impact of inhibiting endosome−lysosome fusion with Bafilomycin A1 (1 nmol/L) pretreatment for 2 h on catabolites produced from the IN and BS T-DM1s with T-DM1 incubation for another 72 h, respectively. (E) Impact of inhibiting cysteine, aspartic and serine protease-dependent proteolytic degradation by treatment with E64d (20 μmol/L), CA-074-ME (3 μmol/L), pepstatin A (20 μg/mL), aprotinin (20 μg/mL) on catabolites produced from the IN and BS T-DM1s after incubation for 72 h in BT474 cells, respectively. The concentrations of the two catabolites, lys-MCC-DM1 and DM1, were quantified by LC–MS/MS ($n = 6$ for each group). All data represent mean ± SEM, $^{*}P < 0.05$, $^{**}P < 0.01$, $^{***}P < 0.001$, Student's *t*-test.

3.3. TARSC analysis of T-DM1s empowers mechanistic studies and biosimilarity assessment

We first measured T-DM1 payloads after the IN T-DM1 administration in BT474 cells. As shown in Fig. 3A, intracellular lys-MCC-DM1 displayed a time-dependent increase, phenocopying the trend of the catabolite, lys-MCC-DM1, produced in CLF. Compared to lys-MCC-DM1, DM1 was present at a pronounced lower concentration upon T-DM1 treatment (Fig. 3A). Moreover, its intracellular concentration and hence its AUC both exhibited a dose−response increase when T-DM1 was administered at 12.5, 25 and 50 nmol/L, whereas that of lys-MCC-DM1 held constant (Fig. 3B). Further, we compared the kinetic profiles of the two T-DM1 catabolites for the IN and BS T-DM1s, and found they both exhibited unequivocal behaviors in target cells BT474 (Fig. 3A and B).

We next applied the TARSC approach to determine how the biological processes initializing from ADC internalization to transport and degradation affect ADC payload kinetics. As antigen binding initializes ADC internalization and the ensuing catabolism[21], we first treated the BT474 cells with HER2 siRNA to suppress HER2 expression. As shown in Fig. 4A, we noted a 48.7% decrease in HER2 expression and concomitantly the

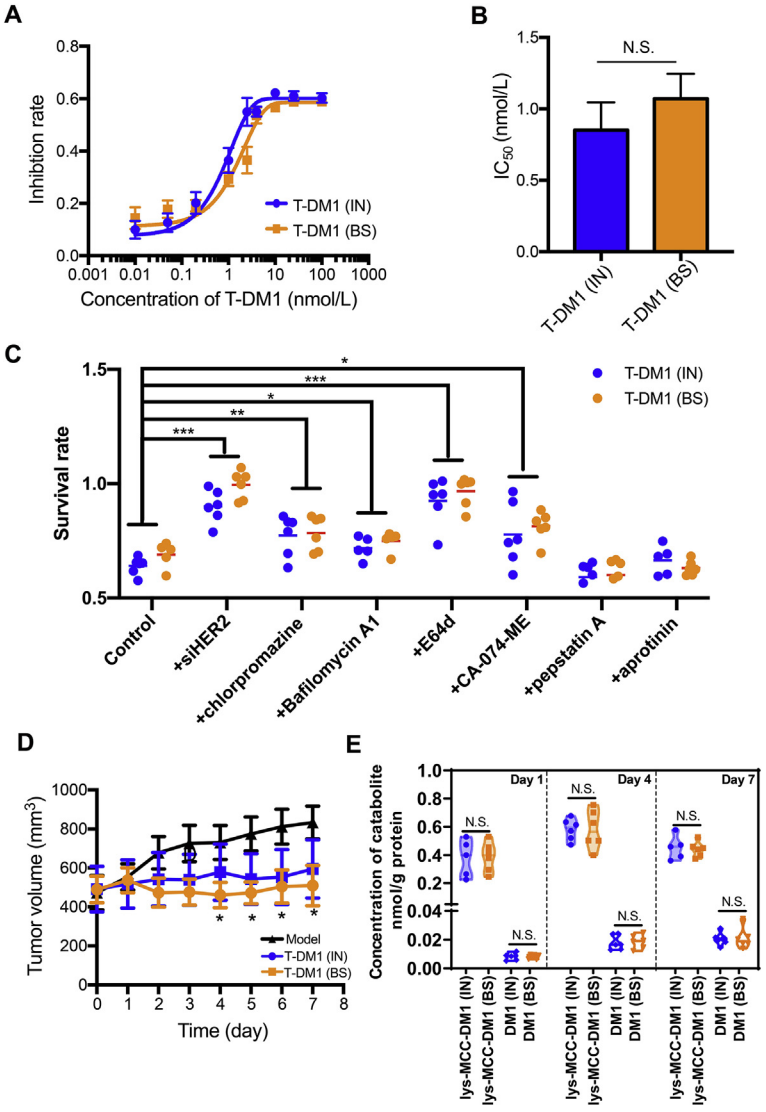

Figure 5 *In vitro* and *in vivo* therapeutic efficacy of the IN and BS T-DM1s. (A) Growth inhibition were measured at 120 h post-administration ($n = 6$). (B) IC_{50} values were compared between the IN and BS T-DM1s. (C) Cell survival rate after the IN and BS T-DM1 treatment subjected to control or targeted interferences. BT474 cells was exposed to 100 nmol/L T-DM1 alone, following 48 h-HER2 silencing or co-administration with 10 μmol/L chlorpromazine, 1 nmol/L Bafilomycin A1, 3 μmol/L CA-074-ME, 20 μmol/L E64d, 20 μg/mL aprotinin or 20 μg/mL pepstatin A as indicated, respectively. At 72 h post-T-DM1 exposure, cell viabilities were measured using a CCK-8 Assay Kit and quantified by comparing the resultant viabilities with those in the absence of indicated treatments. (D) Tumor volumes were measured every day and tumor growth curves were plotted for mice bearing BT474 cell-derived tumor xenografts. (E) The concentrations of intra-tumoral lys-MCC-DM1 and DM1 were measured from the IN and BS T-DM1-treated group, respectively. Specifically, 6 mice from each group were sacrificed at Day 1, 4, 7 post-administration, and the tumors were collected to determine the catabolite concentrations at each assayed time point. All data represent mean ± SEM ($n = 6$). N.S., no significance, *$P < 0.05$, Student's *t*-test for (A), (B), (D), (E) and *$P < 0.05$, **$P < 0.01$, ***$P < 0.001$, one-way ANOVA for (C).

reduced concentration of lys-MCC-DM1 in cells, indicating that disrupted antigen binding indeed leads to impaired ADC payload release. We also tested whether TARSC analysis can be applied to assess the biosimilarity of ADCs, and thus compared the TARSC profile between the BS T-DM1 with its innovator reference. Fig. 4B shows the reduction of intracellular lys-MCC-DM1 exhibited no significant difference between the two, suggesting that HER2 silencing modulated ADC delivery and catabolism to similar extents for both T-DM1s.

Next, since the internalization of cell-surface bound antigen–antibody complex is induced upon antigen binding, we then treated cells with chlorpromazine, an inhibitor of clathrin assembly/disassembly, to interfere with T-DM1 internalization. In line with the clathrin-mediated endocytosis of trastuzumab[22], intracellular concentration of lys-MCC-DM1 following the chlorpromazine treatment shows a significant decrease (Fig. 4C). In addition, the concentration was reduced to comparable levels for both the IN and BS T-DM1-treated cells. Once T-DM1 enters the target cells, it is transported in endosomes to lysosomes. H^+-ATPase is a proton pump present in endosomes and lysosomes, and participates in endosome−lysosome fusion[23,24]. After co-administration of a specific H^+-ATPase inhibitor, Bafilomycin A1, with T-DM1, the aberrant activity of H^+-ATPase in BT474 cells resulted in defected transport of T-DM1 (Fig. 4D).

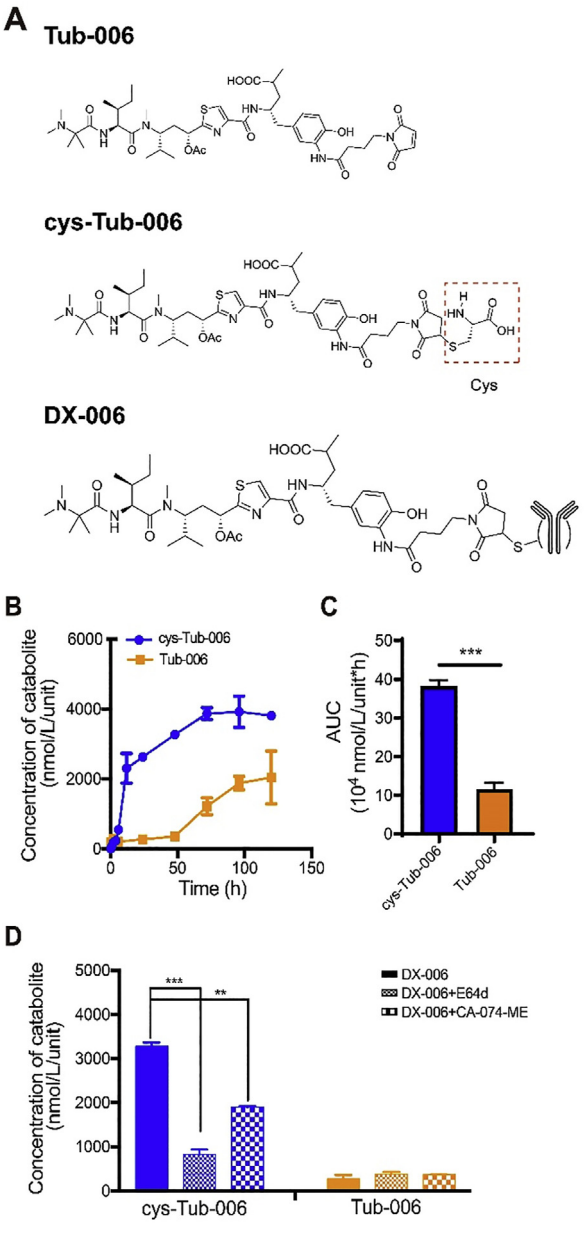

Figure 6 Catabolism profiles of cys-Tub-006 and Tub-006 produced from DX-006 after incubation with rat liver CLF. (A) Schematic illustration of the structure of DX-006. (B) Kinetic profiles of DX-006 catabolites after incubating DX-006 with the crude rat liver lysosomes for 1, 2, 4, 6, 12, 24, 48, 72, 96 and 120 h. (C) AUCs of the detected DX-006 catabolites after lysosomal incubation for 120 h. (D) Lysosomal TARSC analysis of DX-006 achieved by co-administration DX-006 with specific cysteine proteases inhibitors (10 μmol/L E64d, 10 μmol/L CA-074-ME) for 48 h, respectively. All data represent mean ± SEM ($n = 3$), $^{***}P < 0.05$, Student's *t*-test for (C) and $^{**}P < 0.01$, $^{***}P < 0.001$, One-way ANOVA for (D).

Expectedly, the released lys-MCC-DM1 from both the IN and BS T-DM1s was reduced to similar extent (Fig. 4D). Lastly, T-DM1, once being transported into lysosomes, undergoes proteolytic degradation and releases the toxic payloads to induce cancer cell apoptosis. In line with the lysosomal TARSC results, the production of the major catabolite, lys-MCC-DM1, was severely impaired after incubation with the cysteine protease inhibitor E64d (Fig. 4E). The primary contribution of cysteine protease to T-DM1 catabolism is further substantiated by the marked decrease of lys-MCC-DM1 when another cysteine protease inhibitor CA-074-ME was administered. In contrast, neither pepstatin A targeting aspartic protease nor aprotinin targeting serine protease can reduce the yield of lys-MCC-DM1 catabolized from T-DM1 within 72 h post-administration. Collectively, through TARSC analysis of the IN and BS T-DM1 we find TARSC can reveal which protein targets are requisite for ADC payload release and thus lay a mechanistic foundation for advancing ADC R&D by improving the efficiency of ADCs in antigen/mAb binding, internalization, transport and proteolysis. Moreover, TARSC provides a new perspective in biosimilarity assessment, since it examines not only the kinetics of the catabolites in target cells/organelles, but also how the kinetic profiles are influenced in response to targeted interferences.

3.4. TARSC analysis implies in vitro and in vivo therapeutic efficacy

Based on the resemblance of TARSC profiles between the IN and BS T-DM1s, we hence inferred that the two types of T-DM1 would exhibit similar cytotoxicity against BT474 cells. This hypothesis was confirmed in Fig. 5A, which showed that no statistical significance between the IC_{50} values of the IN and BS T-DM1s (Fig. 5B). Next, we asked whether the cytotoxicity of the BS and IN T-DM1 would decrease to similar magnitude when the expression levels of given protein "targets" were diminished or when their functions were impaired. Indeed, we found the *in vitro* viability between the IN and BS T-DM1s both increased upon HER2 silencing, whereas their increases in viability showed no significant difference (Fig. 5C). Similarly, after we inhibited the ADC internalization process *via* chlorpromazine, blocked the transport using Bafilomycin A1 or disrupted lysosomal proteolysis by the administration of E64d and CA-074-ME, significantly diminished *in vitro* potency of both BS and IN T-DM1 were noted compared to that of ADCs subjected to no targeted interferences. In agreement with TARSC analysis, cytotoxicity of both T-DM1s, regardless of the absence or presence of the targeted interferences as exemplified above, held constant. Furthermore, consistent with the negligible effect of aspartic/serine protease inhibition on payload release, inhibition of these proteases using pepstatin A or aprotinin posed no influence on T-DM1-induced cytotoxicity (Fig. 5C). Collectively, the protein targets possibly involved in T-DM1 payload release can be comprehensively tested *via* TARSC analysis, and those that are requisite for payload release and thereby the exertion of anti-cancer efficacy are readily identified.

Furthermore, to examine whether the catabolic behaviors of the two T-DM1s revealed by lysosomal and cellular TARSC study can also be translated to *in vivo* anti-cancer efficacy, we performed a 15 mg/kg single-dose intravenous administration of IN or BS T-DM1 in BT474 xenograft-bearing nude mice and compared the resultant catabolic profiles as well as the anti-tumoral effect. Fig. 5D indicates that both IN and BS T-DM1s exerted significant suppression on tumor growth after 4 days post-treatment. At 7 days post-administration, tumor volumes in the IN and BS T-DM1 treatment groups have shrunk 28.6% and 38.8% compared to the volumes in the control group. No significant difference of the anti-tumor efficacy was observed between the IN and BS T-DM1 treatment.

Lastly, we sought to investigate that whether T-DM1 is catabolized *in vivo* in similar manner as *in vitro* TARSC analysis.

We confirmed that lys-MCC-DM1 is also the major T-DM1 catabolite in tumor mass compared to DM1 (Fig. 5E). Moreover, lys-MCC-DM1 increased in a time-dependent manner at Day 4 compared to Day 1 post-injection. Intriguingly, in agreement with the negligible difference in the concentration of lys-MCC-DM1 within the BT474-xenografted tumors collected at Day 1, 4, and 7 post-administration using the IN and BS T-DM1, no significant difference in the *in vivo* anti-tumoral efficacy was observed between the two T-DM1s (Fig. 5D).

It is thus reasonable to anticipate that TARSC analysis is useful for inferring the *in vitro* and *in vivo* therapeutic efficacy as well as the catabolic behaviors of ADCs during screening. This will significantly assist the judgment regarding whether *in vivo* pharmacological and catabolism experiments should proceed when a plethora of ADC candidates during an early developmental stage need to be analyzed.

3.5. *TARSC analysis of novel ADCs*

A tubulysin ADC-candidate (DX-006) was designed as a cysteine-conjugated noncleavable ADC (Fig. 6A). The linker and warhead were first linked together as Tub-006 and then conjugated to cysteine residues on trastuzumab. The prerequisite for DX-006 to induce significant cancer cell killing effect is the effective release of active toxin upon lysosomal proteolysis. Therefore, we conducted lysosomal TARSC analysis by incubating DX-006 with CLF and measuring the temporal changes of its major catabolites including cys-Tub-006 and Tub-006. As shown in Fig. 6B, we noted both catabolites exhibited a time-dependent increase with prolonged incubation. Moreover, the production of Tub-006 displayed a steeper increase at later time points compared to cys-Tub-006. Since cys-Tub-006 and Tub-006 displayed comparable cytotoxicity against BT474 cells (Supporting Information Fig. S1), the observed kinetics suggest active release of both payloads, and hence predict efficient cell killing effect for DX-006 (Fig. 6C).

We further pursued the catabolism routes of these two catabolized products by incubating DX-006 with selected protease inhibitors. In accordance with other cysteine-conjugated noncleavable ADC, cysteine protease inhibitors blocked the lysosomal catabolism of DX-006 and yielded markedly decreased concentration of cys-Tub-006 in lysosomes (Fig. 6D). Unlike cys-Tub-006, the administration of cysteine proteases inhibitors exhibited negligible influences on the concentration of Tub-006 after incubating DX-006 with CLF.

4. Discussion

In this study, we propose a TARSC approach that measures catabolites kinetics for ADCs of interest, and further examines the changes of the catabolic behaviors in response to pharmacological or genetic interferences posed on given proteins/pathways. We find TARSC is useful for elucidating the requisite proteins involved in ADC delivery and active payload release, and hence the exertion of ADC cytotoxicity. We first investigated the use of TARSC in probing ADC catabolism in lysosomes using the innovator T-DM1 as a model ADC. Indeed, we observed time- and concentration-dependent production of catabolized lys-MCC-DM1 dependent of lysosomal cysteine protease rather than serine/aspartic proteases[25,26]. Previously, *in vitro* studies that aimed to dissect the roles of lysosomal protease in the process of ADC catabolism were conducted using different model systems including enriched lysosomes[25], liver S9 fraction[15] and purified lysosomal protease[27]. However, enzymes contained in liver S9 fractions are much more complicated than lysosomal enzymes, and the microenvironment in liver S9 fractions at pH 7.4 markedly differs from the acidic pH in lysosomes[15,28,29]. Regarding the purified lysosomal proteases, numerous lysosomal enzymes are required to truly mimic the multifarious proteolysis activities that occur within lysosomes[24]. Alternatively, our study employed the easily-harvested CLF from rat liver to monitor the ADC catabolic behaviors, and demonstrated that the CLF competently generated lys-MCC-DM1 in a time-dependent manner as those produced in lysosomes within the target cells BT474 (Supporting Information Fig. S2). In agreement, protein homology analysis of cathepsins show great percentage of identity between those from the two species (Supporting Information Fig. S3), implying their similar structures, functions and comparable activities in protein proteolysis. Therefore, although enriched lysosome fractions collected from target cancer cells can better mimic the release of active payloads occurred in target cells and *in vivo*, the CLF model is believed to serve as a useful system for early-stage screening and quality assessment of ADCs.

After proving TARSC analysis enables ADC catabolism studies in lysosomes, we next asked whether TARSC is applicable to examine the active payloads released from ADCs in intact cells where multiple crucial biological processes including antigen–antibody binding, intracellular internalization, trafficking and lysosomal degradation can be reflected[12,30]. We found that lys-MCC-DM1 did not show dose-dependent increase with the administered concentrations of T-DM1, whereas DM1 increased with the ramped administered concentrations. This distinction in cellular catabolic behaviors can be explained by that the amount of T-DM1 that become internalized and then catabolized to lys-MCC-DM1 already reached saturation at the lowest dose due to the limitedly available amount of HER2 on cell surface, whereas DM1 shed from T-DM1 is directly correlated to the administered dose independent of the amount of unoccupied HER2.

After we obtained the rate and degree of payload released from ADC degradation, we found such information cannot dissect the role of given protein plays in ADC catabolism in target cancer cells. Consequently, similar as lysosomal TARSC, we adopted genetic and pharmacological measures to interfere with certain proteins of interest that we speculated would affect T-DM1 catabolism. We found targeted interferences of HER2, clathrin, H^+-ATPase and lysosomal cysteine protease blocked the release of active payloads, whereas disruption of lysosomal serine and aspartic protease brought negligible changes to T-DM1 catabolism. Thus, TARSC analysis shows potential in identifying proteins that are requisite or conducive to ADC catabolism and hence the exertion of anti-tumoral efficacy. Intriguingly, recent mechanistic study has uncovered a subset of late endolysosomal regulators such as RMC1 that is important for lysosome maturation and consequently ADC toxicity by CRISPR-Cas9 screens[31]. Accordingly, we anticipate the combination of large-scale CRISPR-Cas9 screens with LC–MS/MS-based TARSC analysis can together uncover novel protein targets that regulate ADC internalization, trafficking and payload release, and provide insights regarding how to improve ADC design and propose combination therapeutic strategies.

Notably, in this study we used intracellular concentration of T-DM1 catabolites to estimate how much payloads can access their cytoplasmic targets. Although previous studies and our analysis using tools like LC–MS/MS and fluorimetry have shown that the

majority of payloads once generated in lysosomes escape into the cytosol (Supporting Information Fig. S4), further isolation of cytoplasmic T-DM1 catabolites for TARSC analysis is believed to more accurately reflect the active, free payload that can bind to microtubules located in cytoplasm than intracellular concentration as we adopted for T-DM1 in this study.

Since the therapeutic efficacy of an ADC can only be exerted when its loaded drug is released into its target cells, ADC's catabolic behavior is highly correlated to its therapeutic outcomes[8,32,33]. It is thus reasonable to speculate that TARSC analysis will also deliver useful message for inferring regulators of ADC toxicity. By intervening in proteins essential for ADC internalization, transport and degradation, we demonstrated that the diminished *in vitro* efficacy of ADCs was consistent with the blocked release of T-DM1 catabolites (Fig. 5C). Therefore, the knowledge gained *via* TARSC analysis will significantly improve our understanding of key regulators of not only ADC delivery/catabolism but also the toxicity.

Besides mechanistic studies of ADCs, TARSC opens new avenues for ADC biosimilarity assessment. Specifically, we first conducted lysosomal TARSC analysis using a BS T-DM1, and confirmed that its catabolic profiles, catabolites AUC and the changes in response to targeted interferences of lysosomal protease resembled that of the innovator (Fig. 2). Further, the indistinguishable catabolic behaviors between the IN and BS T-DM1s, regardless of the absence and presence of the specific interferences made to given proteins involved in antigen binding, internalization, transport and degradation, confirmed their biosimilarity. Together with the *in vitro* and *in vivo* anti-tumoral assays, we conclude that the IN and BS T-DM1 were processed and catabolized by its target cells with great biosimilarity, and hence elicited similar toxicity. Thus, our study shows that comparative analysis of ADC TARSC profiles is complementary to the conventional therapeutic efficacy assays such as cytotoxicity that are often employed to evaluate *in vitro* biosimilarity between IN and BS (Fig. 5). Moreover, such information also serves as a valuable reference for inferring similarity regarding *in vivo* efficacy and pharmacokinetics between the ADC IN and BS[34]. However, the *in vitro–in vivo* correlation must be established with discretion[35], since the disposition and catabolism of ADCs *in vivo* is much more complex than that occurring in cultured cells[36,37].

Lastly, TARSC provides clues for ADC design, optimization and screening. For instance, when screening a plethora of ADC candidates composed of different mAbs, linkers or toxins, TARSC elucidates which ADC release the payload rapidly and efficiently, and hence serves as a powerful tool in the discovery stage before proceeding to time-consuming and costly *in vivo* assays. Here we employed lysosomal TARSC to conduct a pilot study on the catabolism of DX-006. We recorded the release of both cys-Tub-006 and Tub-006 in CLF in a time-dependent manner. Intriguingly, the administration of cysteine proteases inhibitors markedly reduced the concentration of cys-Tub-006, whereas the generation of Tub-006 remained unaffected by the administration of lysosomal protease inhibitors. This distinction indicates that the production of cys-Tub-006 necessitates lysosomal cysteine proteases; however, unlike cys-Tub-006, Tub-006 is mainly produced in lysosomes due to retro-Michael addition independent of the examined proteases. Together, the above TARSC results revealed the active release of the two payloads for the new trastuzumab−toxin conjugate in CLF. Such catabolism profile of DX-006 is speculated to lead to improved cytotoxic activity and solicits further scaling-up to *in vivo* efficacy assays.

5. Conclusions

ADCs are embracing an emerging development over the past decade. Versatile combinations of mAb, linker and drug payload have rendered the ADC technology as a powerful drug R&D paradigm that can efficiently reach its target cells with reduced toxicity. Nevertheless, a universal technology that efficiently and conveniently evaluates the involvement of key biological processes in ADC delivery and payload release for mechanistic studies and quality assessment is lacking. Herein, we showed the TARSC approach that measures kinetics of ADC catabolism in target cells and subcellular compartments, and records the changes when given proteins/pathways are genetically or pharmacologically interfered. TARSC can thus be applied to elucidate which proteins such as cysteine or aspartic protease contributes to ADC delivery and degradation for mechanistic studies. Moreover, we demonstrated TARSC analysis can deeply and comprehensively examine the biosimilarity between an ADC biosimilar and its innovator reference. Lastly, the application of lysosomal TARSC analysis to a novel trastuzumab−drug conjugate suggests the active payload release and its catabolism mechanism. Collectively, we anticipate wide and versatile uses of TARSC analysis in ADC early-stage screening, assessment and mechanistic studies, and its strong support to future pharmacological investigations and ADC design/optimization.

Acknowledgments

We acknowledge the financial support of the Natural Science Foundation of Jiangsu Province (BK20180079 and BK20180558, China), the Leading Technology Foundation Research Project of Jiangsu Province (BK20192005, China), the National Natural Science Foundation of China (82173783, 82173882, 81803625), Six Talent Peaks Project in Jiangsu Province (SWYY-101, China), International Industrial Technology Research Collaboration of Nanjing (201911008, China), the Innovative Research Groups of the National Nature Science Foundation of China (81421005), Nantong Science and Technology Project (JC2019133, JCZ18131, China) and the Innovation Team of Affiliated Hospital of Nantong University (TFCT-A05, China).

Author contributions

Study conception and design: Hua Sang, Jiali Liu, Guangji Wang and Hui Ye; Acquisition, analysis and/or interpretation of data: Hua Sang, Jiali Liu, Xiaofang Zhang, Yazhong Liu; Drafting/revision of the work for intellectual content and context: Hua Sang, Jiali Liu, Fang Zhou, Jingwei Zhang and Hui Ye; Final approval and overall responsibility for the published work: Guangji Wang and Hui Ye.

Conflicts of interest

The authors have no conflicts of interest to declare.

Appendix A. Supporting information

Supporting information to this article can be found online at https://doi.org/10.1016/j.apsb.2021.05.024.

References

1. Peters C, Brown S. Antibody–drug conjugates as novel anti-cancer chemotherapeutics. *Biosci Rep* 2015;**35**:e00225.
2. Yan H, Endo Y, Shen Y, Rotstein D, Dokmanovic M, Mohan N, et al. Ado-trastuzumab emtansine targets hepatocytes *via* human epidermal growth factor receptor 2 to induce hepatotoxicity. *Mol Cancer Therapeut* 2016;**15**:480−90.
3. Chari RV, Miller ML, Widdison WC. Antibody–drug conjugates: an emerging concept in cancer therapy. *Angew Chem Int Ed Engl* 2014;**53**:3796−827.
4. Chalouni C, Doll S. Fate of antibody–drug conjugates in cancer cells. *J Exp Clin Cancer Res* 2018;**37**:20.
5. Bargh JD, Isidro-Llobet A, Parker JS, Spring DR. Cleavable linkers in antibody–drug conjugates. *Chem Soc Rev* 2019;**48**:4361−74.
6. Hedrich WD, Fandy TE, Ashour HM, Wang H, Hassan HE. Antibody–drug conjugates: pharmacokinetic/pharmacodynamic modeling, preclinical characterization, clinical studies, and lessons learned. *Clin Pharmacokinet* 2018;**57**:687−703.
7. Lee MV, Kaur S, Saad OM. Conjugation site influences antibody-conjugated drug pk assays: case studies for disulfide-linked, self-immolating next-generation antibody drug conjugates. *Anal Chem* 2020;**92**:12168−75.
8. Beck A, Goetsch L, Dumontet C, Corvaia N. Strategies and challenges for the next generation of antibody–drug conjugates. *Nat Rev Drug Discov* 2017;**16**:315−37.
9. Lyon R. Drawing lessons from the clinical development of antibody–drug conjugates. *Drug Discov Today Technol* 2018;**30**:105−9.
10. Sutherland MS, Sanderson RJ, Gordon KA, Andreyka J, Cerveny CG, Yu C, et al. Lysosomal trafficking and cysteine protease metabolism confer target-specific cytotoxicity by peptide-linked anti-CD-30auristatin conjugates. *J Biol Chem* 2006;**281**:10540−7.
11. Li F, Ulrich M, Jonas M, Stone IJ, Linares G, Zhang X, et al. Tumor-associated macrophages can contribute to antitumor activity through fcγR-mediated processing of antibody–drug conjugates. *Mol Cancer Therapeut* 2017;**16**:1347−54.
12. Lv C, Yang C, Ding D, Sun Y, Wang R, Han D, et al. Endocytic pathways and intracellular transport of aptamer–drug conjugates in live cells monitored by single-particle tracking. *Anal Chem* 2019;**91**:13818−23.
13. Rago B, Tumey LN, Wei C, Barletta F, Clark T, Hansel S, et al. Quantitative conjugated payload measurement using enzymatic release of antibody–drug conjugate with cleavable linker. *Bioconjugate Chem* 2017;**28**:620−6.
14. Kern JC, Cancilla M, Dooney D, Kwasnjuk K, Zhang R, Beaumont M, et al. Discovery of pyrophosphate diesters as tunable, soluble, and bioorthogonal linkers for site-specific antibody–drug conjugates. *J Am Chem Soc* 2016;**138**:1430−45.
15. Bessire AJ, Ballard TE, Charati M, Cohen J, Green M, Lam MH, et al. Determination of antibody–drug conjugate released payload species using directed *in vitro* assays and mass spectrometric interrogation. *Bioconjugate Chem* 2016;**27**:1645−54.
16. Sang H, Lu G, Liu Y, Hu Q, Xing W, Cui D, et al. Conjugation site analysis of antibody–drug-conjugates (ADCs) by signature ion fingerprinting and normalized area quantitation approach using nano-liquid chromatography coupled to high resolution mass spectrometry. *Anal Chim Acta* 2017;**955**:67−78.
17. Liu Y, Zhou F, Sang H, Ye H, Chen Q, Yao L, et al. LC–MS/MS method for the simultaneous determination of Lys-MCC-DM1, MCC-DM1 and DM1 as potential intracellular catabolites of the antibody–drug conjugate trastuzumab emtansine (T-DM1). *J Pharmaceut Biomed Anal* 2017;**137**:170−7.
18. Schroder B, Saftig P. Intramembrane proteolysis within lysosomes. *Ageing Res Rev* 2016;**32**:51−64.
19. Cocchiaro P, Pasquale VD, Morte RD, Tafuri S, Avallone L, Pizard A, et al. The multifaceted role of the lysosomal protease cathepsins in kidney disease. *Front Cell Dev Biol* 2017;**5**:114.
20. He J, Yu S, Yee S, KaurK S, Xu K. Characterization of *in vivo* biotransformations for trastuzumab emtansine by high-resolution accurate-mass mass spectrometry. *mAbs* 2018;**10**:960−7.
21. Singh AP, Guo L, Verma A, Wong GG, Thurber GM, Shah DK. Antibody coadministration as a strategy to overcome binding-site barrier for adcs: a quantitative investigation. *AAPS J* 2020;**22**:28.
22. Wymant JM, Sayers EJ, Muir D, Jones AT. Strategic trastuzumab mediated crosslinking driving concomitant HER2 and HER3 endocytosis and degradation in breast cancer. *J Cancer* 2020;**11**:3288−302.
23. Miao R, Li M, Zhang Q, Yang C, Wang X. An ECM-to-Nucleus signaling pathway activates lysosomes for *C. elegans* larval development. *Dev Cell* 2020;**52**:21−37.e25.
24. Kissing S, Hermsen C, Repnik U, Nesset CK, Bargen KV, Griffiths G, et al. Vacuolar atpase in phagosome–lysosome fusion. *J Biol Chem* 2015;**290**:14166−80.
25. Doronina SO, Mendelsohn BA, Bovee TD, Cerveny CG, Alley SC, Meyer DL, et al. Enhanced activity of monomethylauristatin F through monoclonal antibody delivery: effects of linker technology on efficacy and toxicity. *Bioconjugate Chem* 2006;**17**:114−24.
26. Erickson HK, Park PU, Widdison WC, Kovtun YV, Garrett LM, Hoffman K, et al. Antibody–maytansinoid conjugates are activated in targeted cancer cells by lysosomal degradation and linker-dependent intracellular processing. *Cancer Res* 2006;**66**:4426−33.
27. Dong L, Li C, Locuson C, Chen S, Qian MG. A two-step immunocapture LC/MS/MS assay for plasma stability and payload migration assessment of cysteine-maleimide-based antibody drug conjugates. *Anal Chem* 2018;**90**:5989−94.
28. Niemikoski H, Koske D, Kammann U, Lang T, Vanninen P. Studying the metabolism of toxic chemical warfare agent-related phenylarsenic chemicals *in vitro* in cod liver. *J Hazard Mater* 2020;**391**:122221.
29. Guo J, Wang T, Wu T, Zhang K, Yin W, Zhu M, et al. Synthesis, bioconversion, pharmacokinetic and pharmacodynamic evaluation of *N*-isopropyl-oxy-carbonyloxymethyl prodrugs of CZh-226, a potent and selective PAK4 inhibitor. *Eur J Med Chem* 2020;**186**:111878.
30. Huang Y, Nagro CJ, Balic K, Mylott WR, Ismaiel OA, Ma E, et al. Multifaceted bioanalytical methods for the comprehensive pharmacokinetic and catabolic assessment of MEDI3726, an anti-prostate-specific membrane antigen pyrrolobenzodiazepine antibody–drug conjugate. *Anal Chem* 2020;**92**:11135−44.
31. Tsui CK, Barfield RM, Fischer CR, Morgens DW, Li A, Smith BA, et al. CRISPR-Cas9 screens identify regulators of antibody–drug conjugate toxicity. *Nat Chem Biol* 2019;**15**:949−58.
32. Rios-Luci C, Garcia-Alonso S, Diaz-Rodriguez E, Nadal-Serrano M, Arribas J, Ocana A, et al. Resistance to the antibody–drug conjugate T-DM1 is based in a reduction in lysosomal proteolytic activity. *Cancer Res* 2017;**77**:4639−51.
33. Barok M, Joensuu H, Isola J. Trastuzumab emtansine: mechanisms of action and drug resistance. *Breast Cancer Res* 2014;**16**:209.
34. Pegram MD, Miles D, Tsui CK, Zong Y. HER2-overexpressing/amplified breast cancer as a testing ground for antibody–drug conjugate drug development in solid tumors. *Clin Cancer Res* 2020;**26**:775−86.
35. Shah DK, Loganzo F, Haddish-Berhane N, Musto S, Wald HS, Barletta F, et al. Establishing *in vitro–in vivo* correlation for antibody drug conjugate efficacy: a PK/PD modeling approach. *J Pharmacokinet Pharmacodyn* 2018;**45**:339−49.
36. Haddish-Berhane N, Shah DK, Ma D, Leal M, Gerber HP, Sapra P, et al. On translation of antibody drug conjugates efficacy from mouse experimental tumors to the clinic: a PK/PD approach. *J Pharmacokinet Pharmacodyn* 2013;**40**:557−71.
37. Khera E, Thurber GM. Pharmacokinetic and immunological considerations for expanding the therapeutic window of next-generation antibody–drug conjugates. *BioDrugs* 2018;**32**:465−80.